Effect of off-stoichiometry and Ta doping on Fe-rich $(Mn,Fe)_2(P,Si)$ based giant magnetocaloric materials

Zhang, Fengqi; Batashev, Ivan; van Dijk, Niels; Brück, Ekkes

DOI
10.1016/j.scriptamat.2022.115253

Publication date
2023

Document Version
Final published version

Published in
Scripta Materialia

Scripta Materialia 226 (2023) 115253

Contents lists available at ScienceDirect

Scripta Materialia

journal homepage: www.journals.elsevier.com/scripta-materialia

Effect of off-stoichiometry and Ta doping on Fe-rich $(Mn,Fe)_2(P,Si)$ based giant magnetocaloric materials

Fengqi Zhang [a,*], Ivan Batashev [a,b], Niels van Dijk [a], Ekkes Brück [a]

[a] Fundamental Aspects of Materials and Energy (FAME), Faculty of Applied Sciences, Delft University of Technology, Delft, the Netherlands
[b] Institute for Molecules and Materials, Radboud University, Nijmegen, the Netherlands

ARTICLE INFO

Keywords:
Magnetocaloric effect
$(Mn,Fe)_2(P,Si)$
Off-stoichiometry
Ta doping

ABSTRACT

The influence of off-stoichiometry and of doping with the 5*d* transition metal Ta has been studied in the quaternary $(Mn,Fe)_2(P,Si)$-based compound, which is one of the most promising materials systems for magnetic refrigeration. It is found that Ta substitution can decrease the transition temperature T_{tr}, while the thermal hysteresis ΔT_{hys} remains about constant. A low Ta doping enhances the magnetocaloric effect (MCE). For $Mn_{0.6}Fe_{1.27-y}Ta_yP_{0.64}Si_{0.36}$ with $y = 0.01$ the magnetic entropy change ΔS_m shows and enhancement of 30.7% compared to the undoped material for a low magnetic field change of 1 T. The occupancy of substitutional Ta atoms is determined by XRD and DFT calculations. The T_{tr} shift and enhanced MCE upon Ta doping are ascribed to the competition between a weakening of the magnetic exchange interactions and a strengthening of the hybridization. Our studies provide a good strategy to further optimize the MCE of this material family.

The hexagonal Fe_2P-type $(Mn,Fe)_2(P,Si)$-based magnetocaloric materials (MCMs) demonstrate a giant magnetocaloric effect (GMCE) under low applied magnetic field changes (e.g. 2 T) as a result of the strong magnetoelastic coupling [1,2]. This material family has attracted wide attention because it is rare-earth free, contains no toxic elements, is commercially cheap, shows tunable T_{tr} values and it can be utilized for promising commercial applications like magnetic refrigeration [3], magnetic heat pumps [4] and thermomagnetic generators [5,6].

Different optimization strategies have been proposed to adjust the GMCE performance of $(Mn,Fe)_2(P,Si)$-based MCMs like tuning the metallic (Fe-Mn) and nonmetallic (P-Si) ratios [7,8], chemical pressure engineering (substitutional/interstitial doping) including light elements doping (Li, B, C, N, F, S) [9–12], 3*d* transition metal doping (V, Co, Ni, Cu, Zn) [13–15], 4*d* transition metal doping (Zr, Nb, Mo, Ru) [16–19], other element doping (Al, Ge, As) [20–23] and nano-structuring [24]. Alloying with doping elements does not necessarily only tune the T_{tr} (towards higher T_{tr} - Li, B, C, Al, Ge, Zn and Zr; towards lower T_{tr} - N, F, S, V, Ni, Co, Cu, Ge, Nb, Mo and Ru), but potentially also change the ΔT_{hys}, which is detrimental to the cooling/heating efficiency [25]. Typical doping elements like B, V, Nb and Mo can even shift the strong first-order magnetic transition (FOMT) towards the critical point between the FOMT and the second-order magnetic transition (SOMT) with a negligible ΔT_{hys}, while F doping can make the FOMT stronger with a larger ΔT_{hys}. Effective ways to simultaneous tune T_{tr} and control ΔT_{hys} at a low value are still limited. For most of the non-magnetic elements doping weakens the GMCE in the Mn-Fe-P-Si quaternary alloy system. For the design of active magnetic regenerator (AMR) beds based on MCMs [26], it is crucial to find a strategy to solely regulate T_{tr} and effectively maintain (or improve) the GMCE property without an increase in ΔT_{hys}.

In the present study, at first the impact of off-stoichiometric Fe is studied in Fe-rich $Mn_{0.6}Fe_xP_{0.64}Si_{0.36}$ ($x = 1.19, 1.21, 1.23, 1.25, 1.27, 1.30, 1.35, 1.40$) alloys, where one good candidate ($x = 1.27$) is chosen. Then Ta doping was applied in the $Mn_{0.6}Fe_{1.27-y}Ta_yP_{0.64}Si_{0.36}$ ($y = 0.00, 0.01, 0.02, 0.03, 0.04$) alloys. The Ta doped alloys have been successfully produced and the thermodynamic, GMCE, crystalline structural information has been reported. Doping with the heavy element Ta can effectively tailor T_{tr}, keep ΔT_{hys} constant and increase the GMCE for a low Ta content ($y \leq 0.03$). The Ta atoms are distinguished as substitutional on the 3*g*(Fe) sites by combined X-ray diffraction (XRD) experiments and Density Functional Theory (DFT) calculations. The mechanism responsible for the tunable GMCE properties upon Ta doping is understood from an atomic-scale perspective in terms of the interatomic distances: the shortened intra-layer atomic distances could promote the enhanced *d-d* and *p-d* hybridization among metallic-metallic and metallic-metalloid atoms, respectively. Additionally, the non-

* Corresponding author:.
E-mail address: F.Zhang-7@tudelft.nl (F. Zhang).

https://doi.org/10.1016/j.scriptamat.2022.115253
Received 22 July 2022; Received in revised form 21 November 2022; Accepted 19 December 2022
Available online 30 December 2022

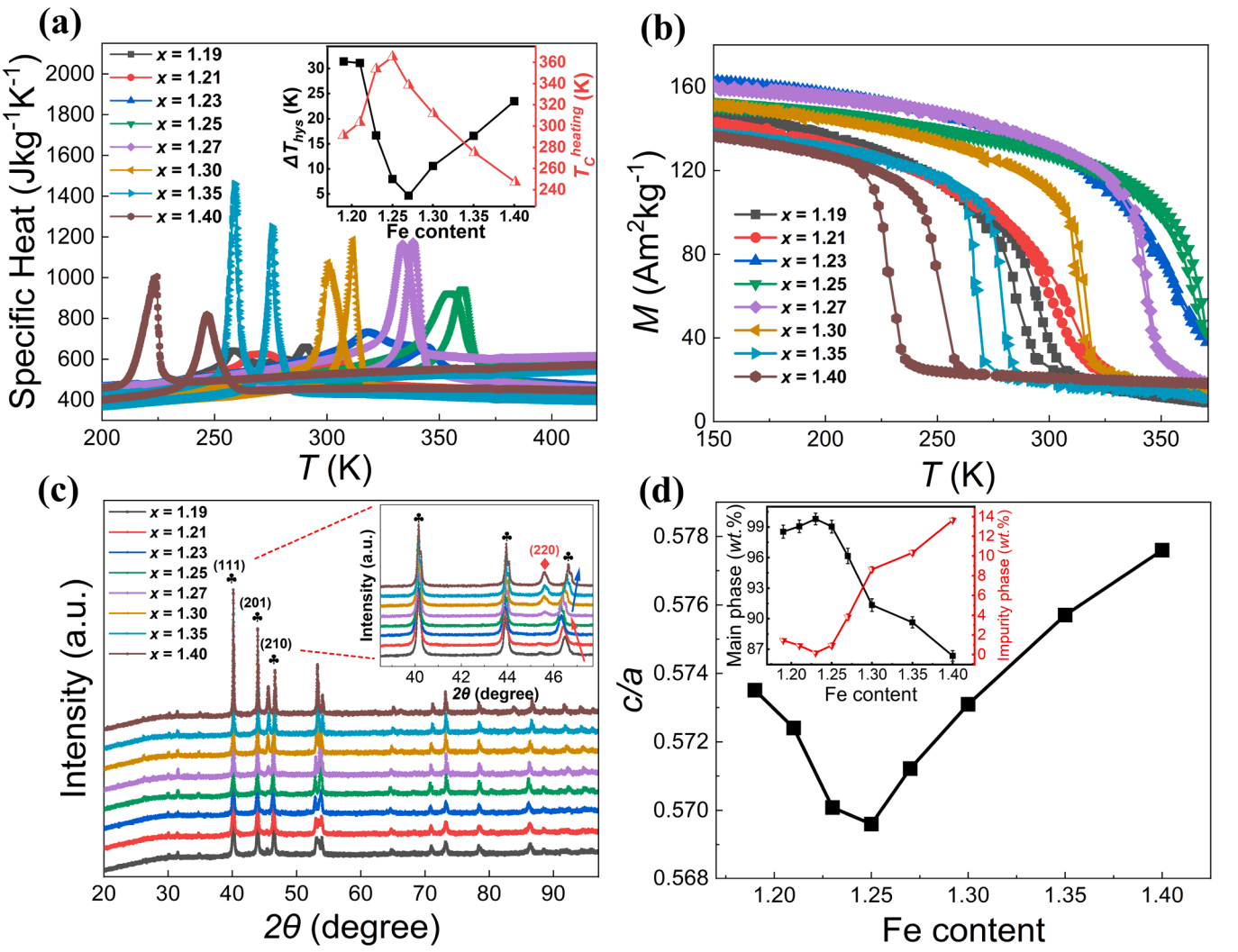

Fig. 1. (a) Specific heat derived from DSC experiments for $Mn_{0.6}Fe_xP_{0.64}Si_{0.36}$ (x = 1.19, 1.21, 1.23, 1.25, 1.27, 1.30, 1.35, 1.40) alloys upon heating and cooling. The inset shows the changes in ΔT_{hys} and $T_{tr}^{heating}$ as function of the Fe content x. (b) Isofield M-T curves for $Mn_{0.6}Fe_xP_{0.64}Si_{0.36}$ (x = 1.19, 1.21, 1.23, 1.25, 1.27, 1.30, 1.35, 1.40) alloys in an applied field of 1 T. (c) The XRD patterns as a function of the Fe content x collected in the high-temperature PM state. The inset shows the main diffraction peaks for different Fe content samples. (d) The derived c/a ratio and phase concentrations as function of the Fe content x.

magnetic Ta atoms replacing Fe on the 3g site, reduce the magnetic exchange interaction. These two effects are expected to be responsible for the shift in T_{tr} and the enhanced GMCE for Ta doped $(Mn,Fe)_2(P,Si)$-based materials. Our current study allows us to further optimize the GMCE by tuning the magnetoelastic coupling by Ta substitution, which may reinforce its potential on magnetic cooling/heating applications.

The off-stoichiometric $Mn_{0.6}Fe_xP_{0.64}Si_{0.36}$ (x = 1.19, 1.21, 1.23, 1.25, 1.27, 1.30, 1.35, 1.40) MCMs and the $Mn_{0.6}Fe_{1.27-y}Ta_yP_{0.64}Si_{0.36}$ (y = 0.00, 0.01, 0.02, 0.03, 0.04) MCMs were synthesized by the solid-state chemical reaction described in a previous paper [24]. To remove the so-called "virgin effect" a pre-cooling process in liquid nitrogen was chosen [27]. Zero-field differential scanning calorimetry (DSC) measurements were carried out using a commercial TA-Q2000 DSC calorimeter (10 K/min), and a home-built Peltier cell-based in-field DSC to derived the ΔS_m and the adiabatic temperature change ΔT_{ad} from specific-heat measurements [28,29]. XRD patterns were collected at a PANalytical X-pert Pro-diffractometer with Cu K_α radiation and analyzed using Fullprof's implementation of the Rietveld refinement method [30]. The temperature-dependent magnetization (M-T) and the field-dependent magnetization (M-H) curves were measured in a superconducting quantum interference device (SQUID, Quantum Design MPMS 5XL) magnetometer. The Vienna *Ab* Initio simulation package (VASP) [31,32] was utilized to conduct DFT calculations within the projector augmented wave method [33,34] with the Perdew-Burke-Ernzerhof (PBE) parametrization [35]. A 2 × 2 × 1 supercell was relaxed with an energy convergence criterion of 1 μeV, a force convergence of 0.1 meV/Å and a kinetic energy cutoff of 400 eV. The site choice for Ta was determined by comparing the formation energies for each possible position $E_f = E_{doped} + \mu_s - (E_{pure} + \mu_{Ta})$ where E_d and E_p are the energies of the doped and the pure compounds, while μ_{Ta} and μ_s are the chemical potentials of Ta and substituted atoms.

To determine the best parent compound for the Ta doping, the off-stoichiometric $Mn_{0.6}Fe_xP_{0.64}Si_{0.36}$ (x = 1.19, 1.21, 1.23, 1.25, 1.27, 1.30, 1.35, 1.40) series of compounds was synthesized. In Fig. 1a, for low Fe contents ($x \leq 1.23$) the endothermic and exothermic peaks significantly decrease in size, and an enlarged spread in T_{tr} may result from an inhomogeneous spatial variation in composition (e.g. shoulder peak for $x = 1.19$ sample). The inset shows the T_{tr} upon heating ($T_{tr}^{heating}$), which first increases and then decreases, and the ΔT_{hys} presents an inverse trend. The inflection point of ΔT_{hys} appears at $x = 1.27$ and the lowest ΔT_{hys} reaches only 4.7 K. As shown in Fig. 1b, the M-T curves indicate that the samples with x = 1.25, 1.27 and 1.30 show a good GMCE performance as they show a high magnetization, a low ΔT_{hys} and a steep slope at T_{tr}. XRD patterns in the paramagnetic (PM) state (T_{tr} +

Table 1
Summary of $T_{tr}^{cooling}$, $T_{tr}^{heating}$, ΔT_{hys}, $dT_{tr}/d\mu_0 H$, the lattice parameters a and c, the c/a ratio, the unit-cell volume V and the concentrations for the main phase and for the $(Mn,Fe)_3Si$ based impurity phase for $Mn_{0.6}Fe_xP_{0.64}Si_{0.36}$ (x = 1.19, 1.21, 1.23, 1.25, 1.27, 1.30, 1.35, 1.40) alloys.

Sample	$T_{tr}^{cooling}$ (K)	$T_{tr}^{heating}$ (K)	ΔT_{hys} (K)	$dT_{tr}/d\mu_0 H$ (K/T)	a (Å)	c (Å)	c/a	V (Å^3)	Main phase *(wt.%)*	Impurity *(wt.%)*
x = 1.19	259.8	291.2	31.4	2.8	6.0230(1)	3.4542(7)	0.5735(1)	108.52(1)	98.6(6)	1.5(2)
x = 1.21	272.5	303.6	31.1	3.5	6.0265(1)	3.4496(7)	0.5724(1)	108.50(1)	99.1(6)	0.9(2)
x = 1.23	337.0	353.7	16.7	3.8	6.0387(1)	3.4425(6)	0.5701(1)	108.72(1)	99.8(6)	0.2(2)
x = 1.25	357.2	365.2	8.0	6.6	6.0381(6)	3.4396(1)	0.5696(1)	108.60(1)	99.1(6)	1.0(2)
x = 1.27	333.9	338.6	4.7	5.0	6.0305(7)	3.4447(5)	0.5712(1)	108.49(1)	96.2(7)	3.8(3)
x = 1.30	301.1	311.7	10.6	3.7	6.0201(7)	3.4501(5)	0.5731(1)	108.29(1)	91.4(6)	8.7(3)
x = 1.35	258.5	275.1	16.6	2.9	6.0071(6)	3.4586(4)	0.5757(1)	108.08(1)	89.7(6)	10.4(2)
x = 1.40	223.8	247.3	23.5	2.3	5.9972(6)	3.4641(4)	0.5776(1)	107.90(1)	86.4(5)	13.7(2)

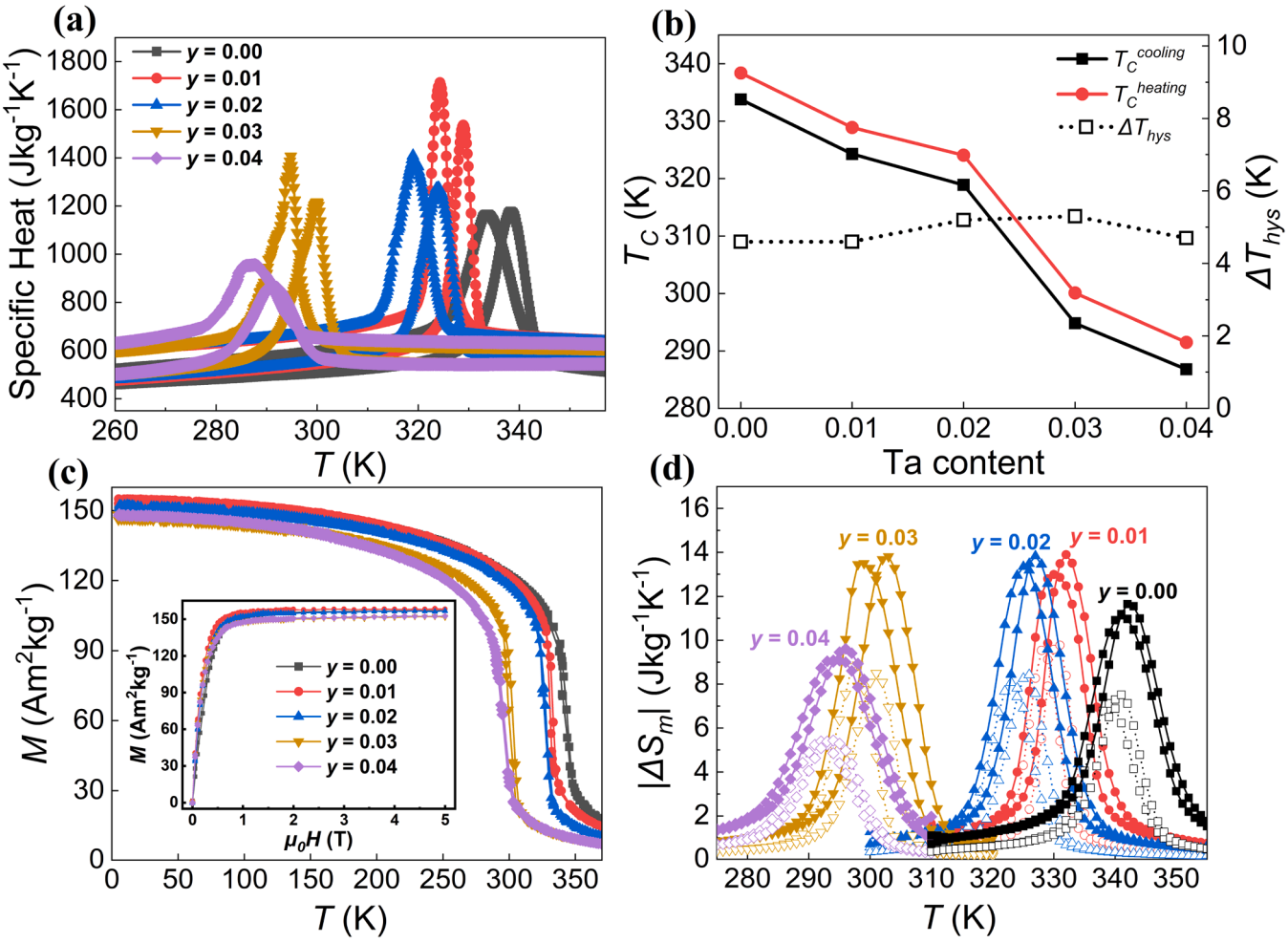

Fig. 2. (a) Specific heat derived from DSC experiments for the $Mn_{0.6}Fe_{1.27-y}Ta_yP_{0.64}Si_{0.36}$ (y = 0.00, 0.01, 0.02, 0.03, 0.04) alloys upon heating and cooling. (b) T_{tr} ($T_{tr}^{heating}$ and $T_{tr}^{cooling}$) and ΔT_{hys} as a function of the Ta doping content y. (c) Isofield M-T curves for the $Mn_{0.6}Fe_{1.27-y}Ta_yP_{0.64}Si_{0.36}$ (y = 0.00, 0.01, 0.02, 0.03, 0.04) alloys. The inset shows the corresponding isothermal M-H curves at 5 K. (d) Magnetic entropy change $|\Delta S_m|$ for $\Delta\mu_0 H$ = 1 T (open symbols) and 2 T (solid symbols) for a varying Ta doping content y.

100°C) are shown in Fig. 1c. The (220) reflection for the $(Mn,Fe)_3Si$ phase has been labelled to indicate the enhanced impurity concentration for the samples with highest Fe content ($x \geq 1.30$). In Fig. 1d the c/a ratio as a function of x shows a similar trend as ΔT_{hys} and a reverse trend as T_{tr}. The c/a ratio is reported to show a close relationship with the magnetic exchange interactions that control the magnetoelastic coupling in Fe_2P-type materials [36,37]. The inset suggests a high main phase fraction ($\geq$ 96 *wt.*%) for $x \leq 1.27$. Therefore, the x = 1.27 composition is selected as parent material for the Ta doping. The parameters like $T_{tr}^{heating}$, $T_{tr}^{cooling}$, ΔT_{hys}, $dT_{tr}/d\mu_0 H$, a, c, c/a, V and the phase concentrations, are summarized in Table 1.

As shown in Fig. 2a, the observed specific heat peaks indicate that the FOMT is maintained upon Ta doping. In Fig. 2b it is clearly observed that the T_{tr} decreases with doping at a rate of dT_{tr}/dy = -11.7 K/at.% Ta. With Ta doping the ΔT_{hys} remains almost constant (about 5 K). This is the first experimental observation of a constant ΔT_{hys} upon doping, which differs from the situation like doping with light elements (B, C, N, F, S) [10–12], doping with 3*d* transition metals (V, Co, Ni, Cu, Zn) [13–15] and doping with 4*d* transition metals (Zr, Nb, Mo, Ru) [16–19] and doping with other elements (Al, Ge, As) [20–23]. However, in comparison to Nb substitution, Ta (r = 1.70 Å) has a comparable covalent radius as Nb (r = 1.64 Å) [38], and therefore generally similar physical properties are

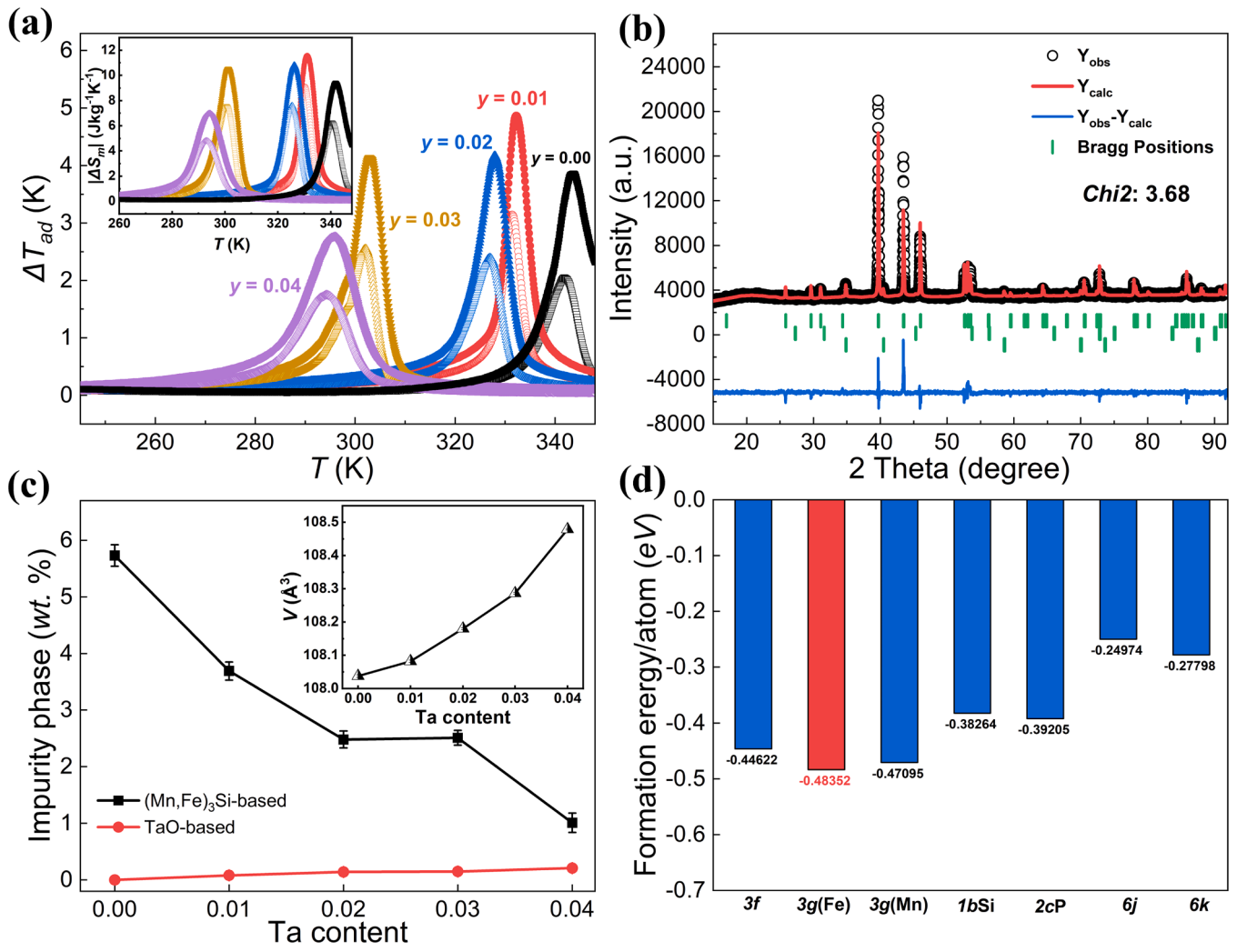

Fig. 3. (a) Derived calorimetric ΔT_{ad} and $|\Delta S_m|$ (inset) obtained from specific heat measurements upon heating for the $Mn_{0.6}Fe_{1.27-y}Ta_yP_{0.64}Si_{0.36}$ (y = 0.00, 0.01, 0.02, 0.03, 0.04) alloys. Note that the open symbols correspond to $\Delta\mu_0 H$ = 1 T and the solid symbols to $\Delta\mu_0 H$ = 1.5 T. (b) Refined XRD pattern for the $Mn_{0.6}Fe_{1.23}Ta_{0.04}P_{0.64}Si_{0.36}$ sample (in the PM state). (c) Derived changes of different phases and unit-cell volume (inset) as function of different Ta contents. (d) Calculated E_f for different site-occupation models of Ta-doped (Mn,Fe)$_2$(P,Si) based materials.

expected as a result of the comparable chemical pressure. The difference between doping with Ta and doping with other 3*d* or 4*d* elements could be ascribed to its unique outer electron configuration ($4f^{14}5d^36s^2$). From Fig. 2c it can be seen that the strong FOMT remains almost constant, while ΔT_{hys} remains small for all samples. For instance, the intrinsic ΔT_{hys} for the y = 0.01 is determined as 2.1 K from Fig. S1b (Supporting Information). The inset indicates only a slight decrease in magnetization at 5 K from 157 Am^2kg^{-1} for y = 0.00 to 152 Am^2kg^{-1} for y = 0.04. Compared with the undoped sample a low Ta doping ($y \leq 0.03$) shows a positive influence on the $|\Delta S_m|$ calculated using the Maxwell relation $\Delta S_m = \int_0^H \left(\frac{\partial M}{\partial T}\right)_H \mu_0 dH$. For y = 0.01 the $|\Delta S_m|$ shows an 31 % (20 %) increase from 7.5(11.6) to 9.8(13.9) $Jkg^{-1}K^{-1}$ for a magnetic field change of $\Delta\mu_0 H$ = 1(2) T. Note that as presented in Fig. S2 (Supporting information) from the 4 successive MCE cycles measurements the reversible $|\Delta S_m|$ is estimated as 8.3(12.5) $Jkg^{-1}K^{-1}$ without any degradation. For y = 0.04 the FOMT character is degraded as $|\Delta S_m|$ reduces to 5.4(9.6) $Jkg^{-1}K^{-1}$ for $\Delta\mu_0 H$ = 1(2) T.

To further evaluate the GMCE performance the values of ΔS_m and ΔT_{ad} have been obtained from a home-built in-field DSC instrument. As illustrated in Fig. 3a, ΔT_{ad} shows an obvious improvement for low Ta contents ($y \leq 0.03$). For y = 0.01 the ΔT_{ad} value increases from 2.0(3.9) to 3.1(4.9) K for $\Delta\mu_0 H$ = 1(1.5) T. The reversible ΔT_{ad} is estimated as 1.8 (2.7) K for $\Delta\mu_0 H$ = 1(2) T based on $\Delta T_{ad} = -\frac{T}{C_p}\Delta S_m^{rev}$, where C_p is zero-field specific heat and ΔS_m^{rev} is the reversible ΔS_m. For y = 0.02 and 0.03 the enhanced ΔT_{ad} are maintained without a significant reduction as they respectively reach 2.4(4.2) and 2.5(4.1) K for $\Delta\mu_0 H$ = 1(1.5) T. This enhancement of ΔT_{ad} is superior to that of the magnetostructural NiMnIn(V) system with $\Delta T_{ad} \approx$ 1.8 K for $\Delta\mu_0 H$ = 1 T [39] and that of the all-*d*-metal NiCoMnTi(B) compound with $\Delta T_{ad} \approx$ 1.1 K for $\Delta\mu_0 H$ = 1 T [40], which also show a good GMCE performance. Note that all the above derived ΔS_m and ΔT_{ad} values are collected at relative low field variations (less than 2 T). This means that these Ta-doped materials are applicable for the current Nd-Fe-B permanent magnets. In the inset the direct measurement values of $|\Delta S_m|$ are shown, which are comparable with the values from the Maxwell relation. The significant increase in $|\Delta S_m|$ for low Ta doping (y = 0.01 – 0.03) further demonstrates that alloying with Ta can not only tailor T_{tr} without influencing ΔT_{hys}, but also results in a larger GMCE. The XRD pattern for the y = 0.04 sample in the high-temperature PM state shown in Fig. 3b has been refined. The refinement indicates the presence of extra (Mn,Fe)$_3$Si based (middle green bar) and TaO based (bottom green bar) impurity phases. In Fig. 3c the (Mn,Fe)$_3$Si based impurity phase shows a drop in concentration from 5.7(2) wt.% for y = 0.00 to 1.0(2) wt.% for y = 0.04 with increasing Ta doping, while the TaO based impurity concentration is low and almost

Table 2
Summary of $T_{tr}^{cooling}$, $T_{tr}^{heating}$, ΔT_{hys}, $dT_{tr}/d\mu_0 H$, lattice parameters a and c, c/a ratio, unit-cell volume V and the phase concentration of the main phase, impurity 2: (Mn, Fe)$_3$Si based phase and impurity 3: TaO based phase for the $Mn_{0.6}Fe_{1.27-y}Ta_yP_{0.64}Si_{0.36}$ (y = 0.00, 0.01, 0.02, 0.03, 0.04) alloys.

Sample	$T_{tr}^{cooling}$ (K)	$T_{tr}^{heating}$ (K)	ΔT_{hys} (K)	$dT_{tr}/d\mu_0 H$ (K/T)	a (Å)	c (Å)	c/a	V (Å^3)	Main (*wt.* %)	Imp 2 (*wt.* %)	Imp 3 (*wt.* %)
y = 0.00	333.8	338.4	4.6	5.0	6.03926 (1)	3.42039 (7)	0.56636 (1)	108.04 (1)	94.3(5)	5.7(2)	0
y = 0.01	324.3	328.9	4.6	4.3	6.02952 (1)	3.43287 (7)	0.56934 (1)	108.08 (1)	96.2(5)	3.7(2)	0.08(1)
y = 0.02	318.9	324.1	5.2	3.5	6.03113 (7)	3.43415 (5)	0.5694(1)	108.18 (1)	97.4(5)	2.5(2)	0.14(1)
y = 0.03	294.8	300.1	5.3	4.4	6.02326 (6)	3.44652 (4)	0.5722(1)	108.29 (1)	97.3(5)	2.5(1)	0.15(1)
y = 0.04	286.8	291.5	4.7	4.4	6.02689 (6)	3.44849 (4)	0.57218 (1)	108.48 (1)	98.8(5)	1.0(2)	0.21(1)

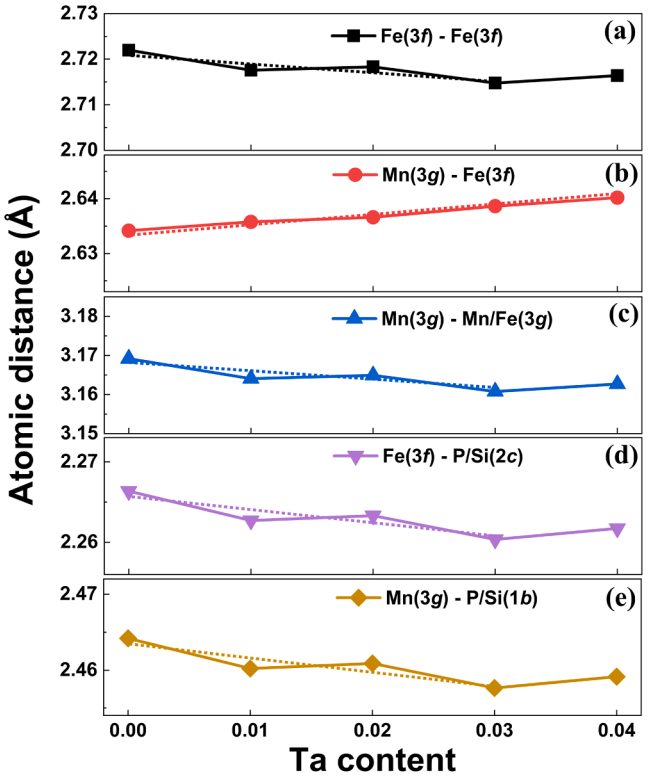

Fig. 4. Interatomic distances of different metallic – metallic pairs (a) Fe(3*f*) – Fe(3*f*), (b) Mn(3*g*) – Fe(3*f*) (c) Mn(3*g*) – Mn/Fe(3*g*), (d) Fe(3*f*) – P/Si(2*c*) and (e) Mn(3*g*) – P/Si(1*b*) for the $Mn_{0.6}Fe_{1.27-y}Ta_yP_{0.64}Si_{0.36}$ (y = 0.00, 0.01, 0.02, 0.03, 0.04) compounds.

constant (0 - 0.2 wt.%). The oxide could be produced because the used Si powder contains a trace amount of SiO_2. It is interesting to note that the concentration of the (Mn,Fe)$_3$Si impurity phase does not significantly change between y = 0.02 and 0.03. The continuous increase in unit-cell volume with Ta doping, as shown in the inset, indicates that the Ta atoms enter the main phase substitutionally as Ta has a bigger atomic covalent radius (r = 1.70 Å) in comparison with Fe (r = 1.32 Å) [38]. Combining these results, suggests that Ta doping has a beneficial effect on the main phase properties (related to the changes of magnetic exchange interaction between magnetic atoms [36]) and leads to a reduction of the (Mn,Fe)$_3$Si impurity phase, which contributes to the systematic shift in T_{tr} with a change in T_{tr} difference between the y = 0.02 and y = 0.03 compounds.

The main parameters for the Ta doped alloys are summarized in Table 2. Precise atomic occupancies for highly ordered crystalline materials is indispensable to characterize their physical properties [11,12,40,41]. Although XRD cannot resolve the occupancy of Mn/Fe (similar structure factors), the position of the heavy element Ta can be uniquely determined at the substitutional 3*g* site. As shown in Fig. 3d, DFT calculations the E_f values of different site-occupation models for Ta-doped (Mn,Fe)$_2$(P,Si) materials clearly suggest that the substitutional 3*g*(Fe) site is the preferential one.

For (Mn,Fe)$_2$(P,Si) MCMs the competition between covalent bonding and ferromagnetic exchange coupling is responsible for the strong GMCE property [42,43]. The reduced T_{tr} indicates the decreased magnetic exchange interaction [44]. However, covalent bonding is also pivotal for the magnetoelastic phase transition [42] and doping with different electronegativity elements can modify its bonding properties [12], and thereby change the band structure for this partially localized and itinerant system [45]. The already distinguished occupancy for the Mn/Fe/P/Si atoms obtained from previous neutron diffraction experiments [11,12,46] and the above DFT calculations make it possible to determine the interatomic distances of different metal – metal pairs using the XRD data, shown in Fig. 4. It is shown that the intra-layer distances gradually decrease for $y \leq 0.03$, while the corresponding distances rise again for y = 0.04. The inter-layer Mn(3*g*) – Fe(3*f*) distances linearly enhance upon Ta doping, as shown in Fig. 4b. Recent experimental investigations on the related (Mn,Fe)$_2$(P,Ge) compounds suggest that the coplanar bonding distances have more effect than the inter-planar distances on the magnetocaloric properties [47]. As a consequence, the shortened intra-layer metallic – metallic and metallic – nonmetallic distances will dominantly contribute to the strengthened *d-d* hybridization among metallic-metallic atoms and *p-d* hybridization among metallic-metalloid atoms due to an increased electron orbital overlap [48]. This effect may compromise the influence of the weakened magnetic exchange interactions among magnetic atoms. Therefore different from other doping cases, the high magnetization and excellent GMCE properties are still maintained after Ta doping. This compromising effect could also result in the degradation of the GMCE for y = 0.04 sample because of its increased atomic distances. Furthermore, as a chemical-twin element for Nb, doping with Ta in the (Mn,Fe)$_2$(P,Si) MCMs behaves completely different from Nb. For example, Nb substitution leads to a continuous reduction in ΔT_{hys} and an attenuated GMCE [17], The difference between Nb and Ta could be ascribed to the difference in electron configuration between Nb ([*Kr*]$4d^4 5s^1$) and Ta ([*Xe*] $4f^{14}5d^3 6s^2$) [49]. Although they contain the same number of valence electrons (e_v = 5), Nb may easier form an effective *p–d* hybridization with metalloids (P/Si) because its 4*d* energy level is markedly lower than the 5*d* energy level, which could lead to a weaker *p–d* hybridization for the Ta doped system and affect the energy barrier of ΔT_{hys}.

In summary, the effect of off-stoichiometric Fe and substitutional Ta doping have been studied for Fe-rich (Mn,Fe)$_2$(P,Si) based MCMs in terms of their basic thermodynamic, magnetic and crystalline structure properties. The Fe content can regulate the T_{tr}, ΔT_{hys} and secondary phase. A high main phase fraction (≥ 96%) in $Mn_{0.6}Fe_xP_{0.64}Si_{0.36}$ alloys values of x = 1.79 - 1.87 should be used for the current production route. Furthermore, Ta substitution solely shifts T_{tr} without influencing ΔT_{hys}. Simultaneously, low Ta doping ($y \leq 0.03$) enhances $|\Delta S_m|$ and ΔT_{ad}. The

Ta atoms are determined to be introduced substitutionally at the 3*g*(Fe) site. The competition between the weakened exchange interactions and the enhanced (*d*-*d* and *p*-*d*) hybridization is expected to be responsible for the unique behavior, including a continuous T_{tr} shift, a constant ΔT_{hys} and an enhanced GMCE.

Declaration of Competing Interest

Non

Acknowledgments

The authors thank Anton Lefering, Bert Zwart, Robert Dankelman and Michel Steenvoorden for their technical assistance. This work was sponsored by NWO in the domain of the Applied and Engineering Sciences (AES) program. Fengqi Zhang gratefully acknowledges financial support from the China Scholarship Council.

Supplementary materials

Supplementary material associated with this article can be found, in the online version, at doi:10.1016/j.scriptamat.2022.115253.

References

[1] O. Tegus, E. Brück, K.H.J. Buschow, F.R. de Boer, Transition-metal-based magnetic refrigerants for room-temperature applications, Nature 415 (2002) 150–152.
[2] N.H. Dung, Z.Q. Ou, L. Caron, L. Zhang, D.T.C. Thanh, G.A. de Wijs, R.A. de Groot, K.H.J. Buschow, E. Brück, Mixed magnetism for refrigeration and energy conversion, Adv. Energy. Mater. 1 (2011) 1215–1219.
[3] E. Brück, Developments in magnetocaloric refrigeration, J. Phys. D. Appl. Phys. 38 (2005) R381–R391.
[4] H. Johra, K. Filonenko, P. Heiselberg, C. Veje, S. Dall'Olio, K. Engelbrecht, C. Bahl, Integration of a magnetocaloric heat pump in an energy flexible residential building, Renew. Energ. 136 (2019) 115–126.
[5] T. Christiaanse, E. Brück, Proof-of-concept static thermomagnetic generator experimental device, Metall. Mater. Trans. E. 1 (2014) 36–40.
[6] A. Waske, D. Dzekan, K. Sellschopp, D. Berger, A. Stork, K. Nielsch, S. Fahler, Energy harvesting near room temperature using a thermomagnetic generator with a pretzel-like magnetic flux topology, Nat. Energy. 4 (2019) 68–74.
[7] N.H. Dung, Moment formation and giant magnetocaloric effects in hexagonal Mn-Fe-P-Si compounds, TU Delft., 2012. PhD. Thesis.
[8] X. You, M. Maschek, N. van Dijk, E. Brück, Magnetic phase diagram of the $Mn_xFe_{2-x}P_{1-y}Si_y$ system, Entropy 24 (2022) 2.
[9] I. Batashev, G.A. de Wijs, N.H. van Dijk, E. Brück, Lithiation of the Fe_2P-based magnetocaloric materials: A first-principles study, J. Magn. Magn. Mater. 537 (2021), 168179.
[10] F. Guillou, G. Porcari, H. Yibole, N. van Dijk, E. Brück, Taming the first-order transition in giant magnetocaloric materials, Adv. Mater. 26 (2014) 2671–2675.
[11] X.F. Miao, N.V. Thang, L. Caron, H. Yibole, R.I. Smith, N.H. van Dijk, E. Brück, Tuning the magnetoelastic transition in $(Mn,Fe)_2(P,Si)$ by B, C, and N doping, Scripta. Mater. 124 (2016) 129–132.
[12] F.Q. Zhang, I. Batashev, Q. Shen, Z.Y. Wu, R.I. Smith, G.A. de Wijs, N. van Dijk, E. Brück, Impact of F and S doping on $(Mn,Fe)_2(P,Si)$ giant magnetocaloric materials, Acta. Mater. 234 (2022), 118057.
[13] J.W. Lai, B.W. Huang, X.F. Miao, N.V. Thang, X.M. You, M. Maschek, L. van Eijck, D.C. Zeng, N. van Dijk, E. Brück, Combined effect of annealing temperature and vanadium substitution for mangetocaloric $Mn_{1.2-x}V_xFe_{0.75}P_{0.5}Si_{0.5}$ alloys, J. Alloy. Compd. 803 (2019) 671–677.
[14] Z.Q. Ou, N.H. Dung, L. Zhang, L. Caron, E. Torun, N.H. van Dijk, O. Tegus, E. Brück, Transition metal substitution in Fe_2P-based $MnFe_{0.95}P_{0.50}Si_{0.50}$ magnetocaloric compounds, J. Alloy. Compd. 730 (2018) 392–398.
[15] X.F. Miao, Zn doped Mn-Fe-P-Si based magnetic refrigeration materials and its preparation method, China. Patent. (2019).
[16] J.T. Feng, F.J. Qian, D.N. Shi, H. Yang, Effect of Zr substitution on the crystal structure, magnetoelastic transition and magnetocaloric properties of $(Mn,Fe)_2(P,Si)$ alloys, Applied. Physics. 9 (2019) 358–364.
[17] S.Y. Hu, X.F. Miao, J. Liu, Z.Q. Ou, M.Q. Cong, O. Haschuluu, Y.Y. Gong, F.J. Qian, Y.R. You, Y.J. Zhang, F. Xu, E. Brück, Small hysteresis and giant magnetocaloric effect in Nb-substituted $(Mn,Fe)_2(P,Si)$ alloys, Intermetallics 114 (2019), 106602.
[18] X.F. Miao, Y. Gong, F.Q. Zhang, Y.R. You, L. Caron, F.J. Qian, W.H. Guo, Y. J. Zhang, Y.Y. Gong, F. Xu, N. van Dijk, E. Brück, Enhanced reversibility of the magnetoelastic transition in $(Mn,Fe)_2(P,Si)$ alloys via minimizing the transition-induced elastic strain energy, J. Mater. Sci. Technol. 103 (2022) 165–176.
[19] H. Wada, K. Nakamura, K. Katagiri, T. Ohnishi, K. Yamashita, A. Matsushita, Tuning the Curie temperature and thermal hysteresis of giant magnetocaloric $(MnFe)_2P_X$ (X = Ge and Si) compounds by the Ru substitution, Jpn. J. Appl. Phys. 53 (2014), 063001.
[20] D.M. Liu, H. Zhang, S.B. Wang, W.Q. Xiao, Z.L. Zhang, N. Tian, C.X. Liu, M. Yue, Q. Z. Huang, J.X. Zhang, J.W. Lynn, The effect of Al doping on the crystal structure and magnetocaloric behavior of $Mn_{1.2}Fe_{0.8}P_{1-x}Ge_x$ compounds, J. Alloy. Compd. 633 (2015) 120–126.
[21] S. Kim, H. Shin, I. Chu, K. Lee, K.H. Lee, W. Lee, Tunable Curie temperature in $Mn_{1.15}Fe_{0.85}P_{0.55}Si_{0.45}$ via lattice engineering by Al addition, J. Alloy. Compd. 890 (2022), 161798.
[22] D.T.C. Thanh, E. Brück, O. Tegus, J.C.P. Klaasse, K.H.J. Buschow, Influence of Si and Ge on the magnetic phase transition and magnetocaloric properties of MnFe(P, Si, Ge), J. Magn. Magn. Mater. 310 (2007) E1012–E1014.
[23] P. Wlodarczyk, L. Hawelek, M. Kowalczyk, M. Kaminska, P. Zackiewicz, M. Polak, M. Hreczka, A. Kolano-Burian, Impact of silicon doping on the magnetocaloric effect of $MnFeP_{0.35}As_{0.65}$ powder, Solid. State. Sci. 56 (2016) 23–28.
[24] F.Q. Zhang, C. Taake, B.W. Huang, X.M. You, H. Ojiyed, Q. Shen, I. Dugulan, L. Caron, N. van Dijk, E. Brück, Magnetocaloric effect in the (Mn,Fe)2(P,Si) system: From bulk to nano, Acta. Mater. 224 (2022), 117532.
[25] L.F. Cohen, Contributions to hysteresis in magnetocaloric materials, Phys. Status. Solidi. B. 255 (2018), 1700317.
[26] B. Huang, J.W. Lai, D.C. Zeng, Z.G. Zheng, B. Harrison, A. Oort, N.H. van Dijk, E. Brück, Development of an experimental rotary magnetic refrigerator prototype, Int. J. Refrig. 104 (2019) 42–50.
[27] X.F. Miao, L. Caron, Z. Gercsi, A. Daoud-Aladine, N.H. van Dijk, E. Brück, Thermal-history dependent magnetoelastic transition in $(Mn,Fe)_2(P,Si)$, Appl. Phys. Lett. 107 (2015), 042403.
[28] G. Porcari, F. Cugini, S. Fabbrici, C. Pernechele, F. Albertini, M. Buzzi, M. Mangia, M. Solzi, Convergence of direct and indirect methods in the magnetocaloric study of first order transformations: The case of Ni-Co-Mn-Ga Heusler alloys, Phys. Rev. B. 86 (2012), 104432.
[29] G. Porcari, M. Buzzi, F. Cugini, R. Pellicelli, C. Pernechele, L. Caron, E. Brück, M. Solzi, Direct magnetocaloric characterization and simulation of thermomagnetic cycles, Rev. Sci. Instrum. 84 (2013), 073907.
[30] H.M. Rietveld, A profile refinement method for nuclear and magnetic structures, J. Appl. Crystallogr. 2 (1969) 65–71.
[31] G. Kresse, J. Hafner, Ab initio molecular dynamics for liquid metals, Phys. Rev. B. 47 (1993) 558–561.
[32] G. Kresse, J. Furthmuller, Efficiency of ab-initio total energy calculations for metals and semiconductors using a plane-wave basis set, Comp. Mater. Sci. 6 (1996) 15–50.
[33] P.E. Blochl, Projector augmented-wave method, Phys. Rev. B. 50 (1994) 17953–17979.
[34] G. Kresse, D. Joubert, From ultrasoft pseudopotentials to the projector augmented-wave method, Phys. Rev. B. 59 (1999) 1758–1775.
[35] J.P. Perdew, K. Burke, M. Ernzerhof, Generalized gradient approximation made simple, Phys. Rev. Lett. 77 (1996) 3865–3868.
[36] E.K. Delczeg-Czirjak, Z. Gercsi, L. Bergqvist, O. Eriksson, L. Szunyogh, P. Nordblad, B. Johansson, L. Vitos, Magnetic exchange interactions in B-, Si-, and As-doped Fe_2P from first-principles theory, Phys. Rev. B. 85 (2012), 224435.
[37] Z. Gercsi, E.K. Delczeg-Czirjak, L. Vitos, A.S. Wills, A. Daoud-Aladine, K. G. Sandeman, Magnetoelastic effects in doped Fe_2P, Phys. Rev. B. 88 (2013), 024417.
[38] B. Cordero, V. Gomez, A.E. Platero-Prats, M. Reves, J. Echeverria, E. Cremades, F. Barragan, S. Alvarez, Covalent radii revisited, Dalton. T. 21 (2008) 2832–2838.
[39] J. Liu, X.M. You, B.W. Huang, I. Batashev, M. Maschek, Y.Y. Gong, X.F. Miao, F. Xu, N. van Dijk, E. Brück, Reversible low-field magnetocaloric effect in Ni-Mn-In-based Heusler alloys, Phys. Rev. Mater. 3 (2019), 084409.
[40] F.Q. Zhang, I. Batashev, N. van Dijk, E. Brück, Reduced hysteresis and enhanced giant magnetocaloric effect in B-Doped all-d-metal Ni-Co-Mn-Ti-based Heusler materials, Phys. Rev. Appl. 17 (2022), 054032.
[41] J.W. Lai, X.M. You, I. Dugulan, B.W. Huang, J. Liu, M. Maschek, L. van Eijck, N. Dijk, E. Brück, Tuning the magneto-elastic transition of $(Mn,Fe,V)_2(P,Si)$ alloys to low magnetic field applications, J. Alloy. Compd. 821 (2020), 153451.
[42] M.F.J. Boeije, P. Roy, F. Guillou, H. Yibole, X.F. Miao, L. Caron, D. Banerjee, N. H. van Dijk, R.A. de Groot, E. Brück, Efficient room-temperature cooling with magnets, Chem. Mater. 28 (2016) 4901–4905.
[43] M. Maschek, X. You, M.F.J. Boeije, D. Chernyshov, N.H. van Dijk, E. Brück, Charge redistribution and the magnetoelastic transition across the first-order magnetic transition in (Mn,Fe)2(P,Si,B), Phys. Rev. B. 98 (2018), 224413.
[44] M. Meinert, J.M. Schmalhorst, G. Reiss, Exchange interactions and Curie temperatures of Mn_2CoZ compounds, J. Phys-Condens. Mat. 23 (2011), 116005.
[45] L. Caron, M. Hudl, V. Hoglin, N.H. Dung, C.P. Gomez, M. Sahlberg, E. Brück, Y. Andersson, P. Nordblad, Magnetocrystalline anisotropy and the magnetocaloric effect in Fe_2P, Phys. Rev. B. 88 (2013), 094440.
[46] X.F. Miao, L. Caron, P. Roy, N.H. Dung, L. Zhang, W.A. Kockelmann, R.A. de Groot, N.H. van Dijk, E. Brück, Tuning the phase transition in transition-metal-based magnetocaloric compounds, Phys. Rev. B. 89 (2014), 174429.
[47] H.R. Zhang, D.M. Liu, Z.L. Zhang, S.B. Wang, M. Yue, Q.Z. Huang, J.W. Lynn, The correlation between the covalent bonds and magnetocaloric properties of the $Mn_{2-x}Fe_xP_yGe_{1-y}M_z$ compounds, J. Appl. Phys. 130 (2021), 133901.
[48] R.H. Petrucci, F.G. Herring, J.D. Madura, General chemistry: principles and modern applications, Prentice. Hall, Pearson, 2010.
[49] N.N. Greenwood, A. Earnshaw, 22-Vanadium, niobium and tantalum. chemistry of the elements, second edition, Butterworth-Heinemann, Oxford, 1997, pp. 976–1001.